IOP PUBLISHING INVERSE PROBLEMS

Inverse Problems **23** (2007) 1801–1819 doi:10.1088/0266-5611/23/5/003

Multi-frequency imaging of multiple targets in Rician fading channels: stability and resolution

Albert C Fannjiang and Pengchong Yan

Department of Mathematics, University of California, Davis, CA 95616-8633, USA

E-mail: fannjiang@math.ucdavis.edu

Received 12 January 2007, in final form 12 June 2007
Published 22 August 2007
Online at stacks.iop.org/IP/23/1801

Abstract

This paper presents an analysis of stability and resolution analysis of broadband (passive or active) array imaging in the Rician fading media. The main theoretical result is the stability condition $KBN \gg M$ where K is the Rician factor, B is the effective number of incoherent frequencies, N is the effective number of array elements and M is the number of sufficiently separated targets. The resolution performance of various imaging functionals is analyzed for the parabolic Markovian model. The imaging method is tested numerically with randomly distributed discrete scatterers. The numerical result with the Foldy–Lax formulation can be matched to the prediction based on the effective medium theory.

(Some figures in this article are in colour only in the electronic version)

1. Introduction

Imaging of obscured targets in random media is a difficult and important problem. One of the central questions is that of stability which is particularly relevant to imaging in stochastic media (see figure 1).

Stability of imaging performance can in principle be improved by increasing the bandwidth of the probing signals and the number of antennas. If the number of targets is one, then counting the degrees of freedom yields the stability condition $B \gg 1$ or $N \gg 1$ where B is the number of independent frequencies and N is the number of independent antennas [2, 3]. In the presence of M targets sufficiently separated in free space, it was shown in [17] that the target locations can be estimated from the one-frequency response matrix when $N \geqslant M$ and multiple scattering among the targets is negligible (see also [6]). A main goal of the paper is to develop a more general criterion for multiple-frequency array imaging of multiple targets in stochastic media.

An important feature of the cluttered medium considered here is that the mean or coherent signals do not vanish. Such is the case for what is called in the wireless literature *Rician fading channel* (medium) where in addition to incoherent signals there is a significant, coherent

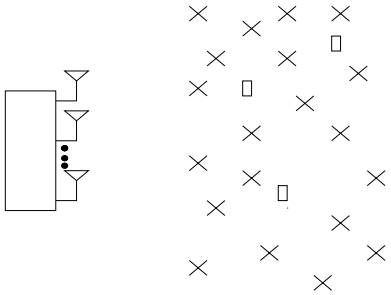

Figure 1. Imaging multiple targets, represented by rectangles, in random media.

component [18]. Typically a Rician channel arises when there is a line of sight between the antennas and the targets. We analyze both passive and active array imaging. In the active case, we focus on the technique of *differential response* which is usually used to detect the *changes* in the media. With proper choices of filters we show that for a Rician fading channel a sufficient condition for imaging stability is $KBN \gg M$ where the Rician factor K is the ratio of signal power in coherent component over the fluctuating power. Under this condition the signal-to-interference ratio (SIR) of the imaging functionals tends to infinity.

The mean-zero case of the Rayleigh fading channels occurs in the diffuse regime which is beyond the scope of the present work. However, it is noteworthy that the above stability condition resembles the stability condition for time reversal *communications* through the Rayleigh fading channels analyzed in [10, 11].

Resolution analysis for the exactly solvable parabolic Markovian model suggests the mean-phase-matched filter which uses only the phase information of the mean transfer function. We test the full imaging process for a discrete model of randomly distributed point scatterers. The imaging result is consistent with the predicted statistical stability. Furthermore, the simulated resolutions can be closely matched to the theoretical resolutions based on the effective medium theory.

The paper is organized as follows. In section 2 we define the notation and the setup of imaging with multiple frequencies and antenna elements, including the passive and active arrays. In section 3 we sketch the argument for the generalized stability condition. As it turns out, the question of stability cannot be separated from that of resolution. Hence in section 4 and appendix A we compare the resolution performances of various commonly used filters for the parabolic Markovian model. This model is analytically most tractable and yields results that may be a guide to more complicated models. In section 5, we discuss the discrete model of randomly distributed point scatterers for which we numerically test the full imaging method. We conclude in section 6.

2. Multi-frequency array imaging

Let $H(\mathbf{x}, \mathbf{y}; \omega)$ be the transfer function (a.k.a. propagator) of the medium at the frequency ω from point $\mathbf{y}$ to $\mathbf{x}$. Denote $H_{mn}(\omega) = H(\mathbf{x}_m, \mathbf{y}_n; \omega)$. Let $\mathbf{H}(\omega) = [H_{mn}(\omega)]$ be the transfer matrix between the antenna located at $\mathbf{y}_n$ and the target located at $\mathbf{x}_m$. The reciprocity implies that $H(\mathbf{y}_n, \mathbf{x}_m; \omega) = H_{mn}(\omega)$. Therefore $\mathbf{H}(\omega)$ is a symmetric matrix and the relation $\mathbf{H}^*(\omega) = \mathbf{H}(-\omega)$ holds where * stands for complex conjugation.

We decompose the random transfer function into the mean $\bar{H}$ and the fluctuation h, $\mathbb{E}h = 0$, as $H(\mathbf{x}, \mathbf{y}; \omega) = \bar{H}(\mathbf{x}, \mathbf{y}; \omega) + h(\mathbf{x}, \mathbf{y}; \omega)$. The mean and fluctuation are also known

as coherent and diffuse fields, respectively. We write $\bar{\mathbf{H}}(\omega) = [\bar{H}_{nm}(\omega)]$ and $\mathbf{h}(\omega) = [h_{mn}(\omega)]$ with $h_{nm}(\omega) = h(\mathbf{x}_m, \mathbf{y}_n; \omega)$.

Our main assumptions are (i) $h_{ij}, \forall\, i, j$, are circularly Gaussian random variables with zero mean; (ii) the separations of the frequencies $\omega_l, l = 1, 2, \ldots, B$ used for imaging are larger than the coherence bandwidth β_c of the cluttered medium; (iii) the spacings of the antennas are wider than the coherence length ℓ_c of the cluttered medium. As a result of these assumptions we have

$$\mathbb{E}\{h_{ij}(\omega_k)h^*_{mn}(\omega_l)\} \approx \eta^2\delta_{im}\delta_{jn}\delta_{k,l}, \qquad \mathbb{E}\{h_{ij}(\omega_k)h_{mn}(\omega_l)\} \approx 0, \qquad \forall\, i, j, m, n, k, l, \tag{1}$$

where η^2 is the intensity of fluctuations. This is of course an idealized condition designed to simplify the presentation (see section 4 and [11] for the discussion of the validity of this approximation).

Let μ be the typical magnitude of the *mean* transfer function and let K be the Rician factor defined as

$$K = \frac{\mu^2}{\eta^2}.$$

Let $u(\mathbf{x})$ be the imaging wave field (to be specified later) which is supposed to exhibit the location and the resolution of the hidden targets. We would like to derive the conditions under which the normalized variance of the imaging wave field u

$$\mathfrak{R}(\mathbf{x}) \equiv \frac{|\mathbb{E}u(\mathbf{x})|^2}{\mathbb{E}(|u|^2(\mathbf{x})) - |\mathbb{E}(u(\mathbf{x}))|^2}$$

tends to infinity at least in the neighborhood of the targets. This is the stability result alluded to earlier. $\mathfrak{R}(\mathbf{x})$ can be viewed as the signal-to-interference ratio (SIR) of the imaging functional at the location $\mathbf{x}$.

To make explicit the imaging field $u(\mathbf{x})$ we divide the discussion into two cases: passive array and active array. We assume that the multiple targets are point scatterers themselves and the interactions among them are negligible (e.g., when they are far apart or their scattering strength is weak compared to the clutter).

2.1. Passive array

First, we consider the case of a passive array in which the targets are sources of multi-frequency signals. The signals are sampled by the antenna array and time reversed (or phase conjugated). The imaging method consists of back-propagating the resulting signals in the computation domain by using an imaging filter $P(\omega)$ which is to be specified later. Let τ_i be the strength of the source $i = 1, \ldots, M$ which is a function of the frequency, i.e. $\tau_i = \tau_i(\omega)$. The resulting wave field is given by

$$u(\mathbf{x}) = \sum_{l=1}^{B}\sum_{j=1}^{N}\sum_{i=1}^{M} \tau_i(\omega_l)P(\mathbf{x}, \mathbf{y}_j; \omega_l)H_{ij}(\omega_l)$$

from which imaging functions can be formed. We write $\mathbf{P}(\omega) = [P_{ij}(\omega)]$ with $P_{ij}(\omega) = P(\mathbf{x}_i, \mathbf{y}_j; \omega)$. For simplicity we assume identical sources, i.e. $\tau_i(\omega) = \tau(\omega), \forall\, i$.

2.2. Active array

In the case of an active array, we consider the method of the *differential response*. In this approach, probing signals of various frequencies are first used to survey the random media

in the absence of targets. Then in the presence of targets (with unknown locations) the same set of probing signals is used again to survey the media which are assumed to be fixed. The difference between these two responses is called the differential response which is then used to image the targets. The advantage with differential response is that the medium uncertainty is reduced by subtracting the clutter response (without the targets) as we are only interested in the change (i.e., the inclusion of the targets) in the cluttered medium.

Let τ_i be the scattering strength (reflectivity) of the ith target, $i = 1, \ldots, M$. In general, τ_i is a function of the frequency $\tau_i = \tau_i(\omega)$, see (23) below. We shall assume weakly scattering targets so that the multiple scattering between the targets and the clutter is negligible and the only multiple scattering effect is in the clutter. In this approximation, the differential responses are given by $\sum_{i=1}^{M} \tau_i(\omega_l) H_{ij}(\omega_l) H_{in}(\omega_l)$, $j = 1, \ldots, N, l = 1, \ldots, B$ where the index $n = 1, \ldots, N$ indicates the array elements emitting the probing signals. The imaging field in this case is given by

$$u(\mathbf{x}) = \sum_{l=1}^{B} \sum_{i=1}^{M} \sum_{j,n=1}^{N} \tau_i(\omega_l) P(\mathbf{x}, \mathbf{y}_j; \omega_l) H_{ij}(\omega_l) H_{in}(\omega_l) P(\mathbf{y}_n, \mathbf{x}; \omega_l).$$

For simplicity, we assume identical targets, i.e. $\tau_i(\omega) = \tau(\omega), \forall\, i$.

3. Stability condition: proof of concept

In this section we derive for the Rician channels the stability condition $KBN \gg M$. Under this stability condition the imaging field $u(\mathbf{x})$ is approximately equal to its mean $\mathbb{E}u(\mathbf{x})$.

3.1. Passive array

Let us calculate the mean. We have

$$\mathbb{E}u(\mathbf{x}) = \sum_{i=1}^{M} \sum_{l=1}^{B} \sum_{j=1}^{N} \tau(\omega_l) P(\mathbf{x}, \mathbf{y}_j; \omega_l) \bar{H}_{ij}(\omega_l) = O(\mu BN). \tag{2}$$

The apparent missing factor M in the above estimate is due to the choice of a suitable filter for the purpose of resolution enhancement. Ideally, in the case of point targets, we would like to have $\mathbb{E}u(\mathbf{x})$ as a sum of delta-like functions centered at the M sufficiently separated targets. As a consequence of the sharp localization of the delta-like functions, there are effectively only $O(1)$ terms in the summation over i independent of M. On the other hand, as we will see in (3), the fluctuations increase with M. In other words, for large $M \gg 1$, the resolution comes at the price of statistical stability.

Next, we calculate the variance of u. We have

$$\begin{aligned}
\mathbb{E}|u(\mathbf{x})|^2 = \mathbb{E} \Bigg\{ & \sum_{l=1}^{B} \sum_{j=1}^{N} \sum_{i=1}^{M} \tau(\omega_l) P(\mathbf{x}, \mathbf{y}_j; \omega_l) H_{ij}(\omega_l) \\
& \times \sum_{l'=1}^{B} \sum_{j'=1}^{N} \sum_{i'=1}^{M} \tau^*(\omega_{l'}) P^*(\mathbf{x}, \mathbf{y}_{j'}; \omega_{l'}) H^*_{i'j'}(\omega_{l'}) \Bigg\} \\
= & \sum_{l,l'=1}^{B} \sum_{i,i'=1}^{M} \sum_{j,j'=1}^{N} \tau(\omega_l) \tau^*(\omega_{l'}) P(\mathbf{x}, \mathbf{y}_j; \omega_l) \bar{H}_{ij}(\omega_l) P^*(\mathbf{x}, \mathbf{y}_{j'}; \omega_{l'}) \bar{H}^*_{i'j'}(\omega_{l'})
\end{aligned}$$

$$+\sum_{l=1}^{B}\sum_{j=1}^{N}\sum_{i=1}^{M}|\tau(\omega_l)|^2\,\mathbb{E}\{P(\mathbf{x},\mathbf{y}_j;\omega_l)h_{ij}(\omega_l)P^*(\mathbf{x},\mathbf{y}_j;\omega_l)h_{ij}^*(\omega_l)\}$$

$$\approx |\mathbb{E}u(\mathbf{x})|^2+\eta^2 M\sum_{l=1}^{B}\sum_{j=1}^{N}|\tau(\omega_l)|^2|P(\mathbf{x},\mathbf{y}_j;\omega_l)|^2(\omega_l)$$

$$=|\mathbb{E}u(\mathbf{x})|^2+O(\eta^2 BMN). \tag{3}$$

It follows from (2) and (3) that $\mathfrak{R}\to\infty$ as $KBN\gg M$.

3.2. Active array

The expectation of u is then given by

$$\mathbb{E}u(\mathbf{x})=\sum_{l=1}^{B}\sum_{i=1}^{M}\sum_{j,n=1}^{N}\tau(\omega_l)P(\mathbf{x},\mathbf{y}_j;\omega_l)(\bar{H}_{ij}\bar{H}_{in}(\omega_l)+\mathbb{E}[h_{ij}h_{in}(\omega_l)])P(\mathbf{y}_n,\mathbf{x};\omega_l)$$

$$\approx\sum_{l=1}^{B}\sum_{i=1}^{M}\sum_{j,n=1}^{N}\tau(\omega_l)P(\mathbf{x},\mathbf{y}_j;\omega_l)\bar{H}_{ij}\bar{H}_{in}(\omega_l)P(\mathbf{y}_n,\mathbf{x};\omega_l)$$

$$=O(\mu^2 BN^2). \tag{4}$$

Again, the apparent missing factor M in the above estimate is due to the choice of suitable filter P to achieve resolution so that we can only expect $O(1)$ terms in the above summation over i.

Note that here the expression for u contains a *product* of $\mathbf{H}$, in contrast to the passive case. As a result, the expectation of u involves the second order moments of h and the variance of u involves the fourth order moments of h. In calculation of the fourth order moments we shall adopt the rule of Gaussian statistics. The fourth order Gaussian model is widely used and includes the Rician and Rayleigh fading channels in wireless modeling [8, 18].

Using the Gaussian rule for the fourth order moments we obtain

$$\mathbb{E}|u(\mathbf{x})|^2\approx\left|\sum_{l=1}^{B}\sum_{i=1}^{M}\sum_{j,n=1}^{N}\tau(\omega_l)P(\mathbf{x},\mathbf{y}_j;\omega_l)\bar{H}_{ij}\bar{H}_{in}(\omega_l)P(\mathbf{y}_n,\mathbf{x};\omega_l)\right|^2$$

$$+\mathbb{E}\left\{\left|\sum_{l=1}^{B}\sum_{i=1}^{M}\sum_{j,n=1}^{N}\tau(\omega_l)P(\mathbf{x},\mathbf{y}_j;\omega_l)(\bar{H}_{ij}h_{in}(\omega_l)+h_{ij}\bar{H}_{in}(\omega_l))P(\mathbf{y}_n,\mathbf{x};\omega_l)\right|^2\right\}$$

$$+\mathbb{E}\left\{\left|\sum_{l=1}^{B}\sum_{i=1}^{M}\sum_{j,n=1}^{N}\tau(\omega_l)P(\mathbf{x},\mathbf{y}_j;\omega_l)h_{ij}h_{in}(\omega_l)P(\mathbf{y}_n,\mathbf{x};\omega_l)\right|^2\right\}$$

which becomes after applying (1)

$$\mathbb{E}|u(\mathbf{x})|^2\approx|\mathbb{E}u(\mathbf{x})|^2+2\eta^2\sum_{l=1}^{B}\sum_{i=1}^{M}\sum_{j,n,n'=1}^{N}|\tau(\omega_l)|^2|P(\mathbf{x},\mathbf{y}_j;\omega_l)|^2$$

$$\times\bar{H}_{in}P(\mathbf{y}_n,\mathbf{x};\omega_l)\bar{H}_{in'}^*P^*(\mathbf{y}_{n'},\mathbf{x};\omega_l)$$

$$+2\eta^2\sum_{l=1}^{B}\sum_{i=1}^{M}\sum_{j,n,n'=1}^{N}|\tau(\omega_l)|^2P(\mathbf{x},\mathbf{y}_j;\omega_l)\bar{H}_{ij}(\omega_l)$$

$$\times P(\mathbf{y}_n, \mathbf{x}; \omega_l) P^*(\mathbf{x}, \mathbf{y}_n; \omega_l) \bar{H}^*_{in'}(\omega_l) P^*(\mathbf{y}_{n'}, \mathbf{x}; \omega_l)$$
$$+ \eta^4 M \sum_{l=1}^{B} \sum_{j,n=1}^{N} |\tau(\omega_l)|^2 (|P(\mathbf{x}, \mathbf{y}_j; \omega_l)|^2 |P(\mathbf{y}_n, \mathbf{x}; \omega_l)|^2$$
$$+ P(\mathbf{x}, \mathbf{y}_j; \omega_l) P^*(\mathbf{y}_j, \mathbf{x}; \omega_l) P^*(\mathbf{x}, \mathbf{y}_n; \omega_l) P(\mathbf{y}_n, \mathbf{x}; \omega_l)).$$

Note that the last term in (5) is $O(\eta^4 BMN^2)$. Hence

$$\mathbb{E}|u(\mathbf{x})|^2 \approx |\mathbb{E}u(\mathbf{x})|^2 + O(\eta^2 \mu^2 BMN^3 + \eta^4 BMN^2). \tag{5}$$

Therefore, for an active array and in the regime that KN is bounded away from zero we have $\mathfrak{R} \to \infty$ when $KBN \gg M$.

An useful result here for the subsequent analysis is (2), for the passive imaging, and (4), for the active imaging, which are the theoretical foundation of resolution of our imaging process.

4. Parabolic Markovian model

The principal ingredients of the clutter model in our approach are the coherence bandwidth β_c and length ℓ_c. Here we describe the parabolic Markovian model for which the coherent field, β_c and ℓ_c, can be estimated or numerically computed.

This model is for a random continuum widely used for light propagation in the atmospheric turbulence where the refractive index n is a continuously varying random function in space [14]. In the long-distance propagation regime, the index fluctuation $\tilde{n}$ can be treated as a white-noise process in the propagation direction

$$\mathbb{E}(\tilde{n}(z, \mathbf{x}^\perp)\tilde{n}(z', \mathbf{y}^\perp)) = \delta(z - z')C(z, \mathbf{x}^\perp, \mathbf{y}^\perp),$$

where $z \in \mathbb{R}$ and $\mathbf{x}^\perp \in \mathbb{R}^{d-1}, d = 2, 3$, are the longitudinal and transverse coordinates, respectively, of the cluttered medium, and C is the correlation function. We shall write $\tilde{n}(z, \mathbf{x}^\perp) = \mathrm{d}V_z(\mathbf{x}^\perp)$ where V_z is a Wiener process in a suitable function space.

In the parabolic approximation the beam wave modulation $\Psi(z, \mathbf{x}^\perp)$ with the carrier wavenumber $\bar{k}$ is described by the following stochastic Schrödinger–Itô equation [14]:

$$d_z \Psi(z, \mathbf{x}^\perp) = \frac{\mathrm{i}}{2\bar{k}} \triangle^\perp \Psi(z, \mathbf{x}^\perp)\, \mathrm{d}z - \frac{\bar{k}^2}{2} C(z, \mathbf{x}^\perp, \mathbf{x}^\perp) \Psi(z, \mathbf{x}^\perp)\, \mathrm{d}z + \mathrm{i}\bar{k} \Psi(z, \mathbf{x}^\perp)\, \mathrm{d}V_z(\mathbf{x}^\perp). \tag{6}$$

Note that here $\bar{k}$ is the effective wavenumber which is the effective index of refraction $\bar{n}$ (usually larger than 1) times the free-space wavenumber k. In what follows we adopt the space-time units so that the effective wave speed is unity and thus the effective wavenumber $\bar{k}$ equals the free-space frequency ω. It is clear from (6) that the mean propagator $\bar{H}$ is $\mathrm{e}^{\mathrm{i}\omega z}$ times the Green function of the operator

$$\frac{\partial}{\partial z} - \frac{\mathrm{i}}{2\omega} \triangle^\perp + \omega^2 C(z, \mathbf{x}^\perp, \mathbf{x}^\perp)/2. \tag{7}$$

With the knowledge of C (from channel estimation) the mean propagator can be easily solved by numerical methods. To simplify the discussion and presentation let us make the assumption of statistical homogeneity of $\tilde{n}$ such that $C(z, \mathbf{x}^\perp, \mathbf{y}^\perp) = C(\mathbf{x}^\perp - \mathbf{y}^\perp)$. Then the mean propagator is given explicitly by

$$\bar{H}(z, \mathbf{x}^\perp, \mathbf{y}^\perp; \omega) = \frac{\omega^{d/2}}{(2\pi \mathrm{i} z)^{d/2}} \mathrm{e}^{-\omega^2 C(0) z/2} \mathrm{e}^{-\mathrm{i}\omega z} \mathrm{e}^{\mathrm{i}\frac{\omega |\mathbf{x}^\perp - \mathbf{y}^\perp|^2}{2z}}. \tag{8}$$

The coherence length ℓ_c and bandwidth β_c can be determined from the field-to-field correlations. Let Γ be the two-frequency covariance function

$$\Gamma\big(z, \mathbf{x}_1^\perp, \mathbf{x}_2^\perp; \omega_1, \omega_2\big) = \mathbb{E}\big[\Psi\big(z, \mathbf{x}_1^\perp; \omega_1\big)\Psi^*\big(z, \mathbf{x}_2^\perp; \omega_2\big)\big] - \mathbb{E}\Psi\big(z, \mathbf{x}_1^\perp; \omega_1\big)\mathbb{E}\Psi^*\big(z, \mathbf{x}_2^\perp; \omega_2\big),$$

which satisfies the equation [14]

$$\frac{\partial}{\partial z}\Gamma = \imath\left(\frac{1}{2\omega_1}\triangle_1^\perp - \frac{1}{2\omega_2}\triangle_2^\perp\right)\Gamma - \frac{|\omega_1-\omega_2|^2}{2}C(0)\Gamma - \omega_1\omega_2 D\big(\mathbf{x}_2^\perp - \mathbf{x}_1^\perp\big)\Gamma$$
$$+\omega_1\omega_2 C\big(\mathbf{x}_1^\perp - \mathbf{x}_2^\perp\big)\mathbb{E}\Psi\big(z,\mathbf{x}_1^\perp;\omega_1\big)\mathbb{E}\Psi^*\big(z,\mathbf{x}_2^\perp;\omega_2\big), \tag{9}$$

where $D(\mathbf{x}^\perp) = C(0) - C(\mathbf{x}^\perp) \geqslant 0$ is the structure function of the media. The covariance function is also known as the *incoherent* part of the mutual coherence function while $\mathbb{E}\Psi\big(z,\mathbf{x}_1^\perp;\omega_1\big)\mathbb{E}\Psi^*\big(z,\mathbf{x}_2^\perp;\omega_2\big)$ is the coherent part of the mutual coherence function [14].

Clearly from equation (9) it follows that as $\omega' = \omega_1 - \omega_2$ increases Γ decays at least as fast as $\exp(-|\omega'|^2 C(0)z/2)$ which would yield the upper bound $\beta_c \leqslant (C(0)z)^{-1/2}$. For the weak fluctuation concerning us here, the equation can be solved approximately by the Rytov method [14]. In the high-frequency, strong-fluctuation regime the sharp estimate $\beta_c \sim |D''(0)|^{-1}z^{-2}$ can be obtained where D'' is the second derivative of D in the isotropic case [9, 11]. Likewise, ℓ_c can be determined from equation (9) with $\omega_1 = \omega_2 = \omega$. This yields for the point source located at $\mathbf{y} = 0$ the following estimate [12]

$$\begin{aligned}\Gamma\big(z,\mathbf{x}_1^\perp,\mathbf{x}_2^\perp;\omega,\omega\big) &\approx \bar{H}\big(z,\mathbf{x}_1^\perp,0;\omega\big)\bar{H}^*\big(z,\mathbf{x}_2^\perp,0;\omega\big)\\ &\quad\times\left[\exp\left(-\omega^2 z\int_0^1 C\big(\big(\mathbf{x}_2^\perp-\mathbf{x}_1^\perp\big)s\big)\,\mathrm{d}s\right)-1\right]\\ &\approx \bar{H}\big(z,\mathbf{x}_1^\perp,0;\omega\big)\bar{H}^*\big(z,\mathbf{x}_2^\perp,0;\omega\big)\\ &\quad\times\left[\exp\left(-\omega^2 z\left(1-\frac{1}{6}D''(0)\big|\mathbf{x}_2^\perp-\mathbf{x}_1^\perp\big|^2\right)\right)-1\right].\end{aligned}$$

It follows that

$$\ell_c \sim \frac{1}{\omega\sqrt{D''(0)z}}.$$

We emphasize here that ℓ_c and β_c can be determined from *statistical* quantities such as $C(0)$ and $D''(0)$ which can be reasonably measured.

Let us now consider four different filters and study the respective mean imaging field $\mathbb{E}u(\mathbf{x})$ in the passive mode:

(i) the mean-matched filter,

$$P(z,\mathbf{x}^\perp,\mathbf{y}^\perp;\omega_l) = \frac{\omega_l^{d/2}}{(2\pi\mathrm{i}z)^{d/2}}\,\mathrm{e}^{-\omega_l^2 C(0)z/2}\,\mathrm{e}^{\mathrm{i}\omega_l z}\,\mathrm{e}^{-\mathrm{i}\frac{\omega_l|\mathbf{x}^\perp-\mathbf{y}^\perp|^2}{2z}}, \qquad l=1,\ldots,B, \tag{10}$$

(ii) the mean-phase-matched filter,

$$P(z,\mathbf{x}^\perp,\mathbf{y}^\perp;\omega_l) = \mathrm{e}^{\mathrm{i}\omega_l z}\,\mathrm{e}^{-\mathrm{i}\frac{\omega_l|\mathbf{x}^\perp-\mathbf{y}^\perp|^2}{2z}}, \qquad l=1,\ldots,B, \tag{11}$$

(iii) the free-space parabolic propagator,

$$P(z,\mathbf{x}^\perp,\mathbf{y}^\perp;\omega_l) = \frac{\omega_l^{d/2}}{(2\pi\mathrm{i}z)^{d/2}}\,\mathrm{e}^{\mathrm{i}\omega_l z}\,\mathrm{e}^{-\mathrm{i}\frac{\omega_l|\mathbf{x}^\perp-\mathbf{y}^\perp|^2}{2z}}, \qquad l=1,\ldots,B, \tag{12}$$

(iv) the mean inverse filter,

$$P(z,\mathbf{x}^\perp,\mathbf{y}^\perp;\omega_l) = \frac{\omega_l^{d/2}}{(2\pi\mathrm{i}z)^{d/2}}\,\mathrm{e}^{\omega_l^2 C(0)z/2}\,\mathrm{e}^{\mathrm{i}\omega_l z}\,\mathrm{e}^{-\mathrm{i}\frac{\omega_l|\mathbf{x}^\perp-\mathbf{y}^\perp|^2}{2z}}, \qquad l=1,\ldots,B. \tag{13}$$

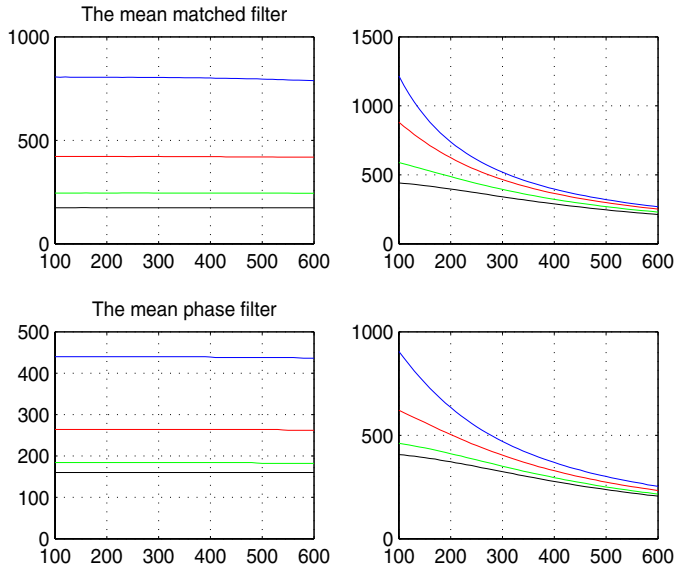

Figure 2. Longitudinal (left column) and transverse (right column) resolution of the parabolic Markovian model with the matched and phase-matched filters with various extinction coefficients. The blue (full), red (dashed), green (dotted) and black (chain) curves represent, respectively, $C(0) = 0.16, 0.08, 0.04, 0.02$. The horizontal axis denotes the antenna spacing with five antennas. The resolution is defined as the distance from the target where the value $|\mathbb{E}u|$ has dropped to the half of its target value.

All the above filters have the same phase function with the only differences being the range-dependent factor and the frequency-weight function. Approximate calculations with these filters are given in the appendix. As we see there, all four filters result in the order of magnitude as given in (2). The transverse resolutions of all of the first three filters have the same scaling behavior $\sqrt{C(0)z_1^3}$ where z_1 is the range. In contrast, the mean inverse filter has a transverse resolution which is independent of $C(0)$ but inversely depends on the total bandwidth $B\beta_c$.

To compare them numerically (see figures 2 and 3), we use a linear array of five equally spaced antennas, lying on the plane $z = -5000$, and 20 equally spaced wavelengths (to avoid aliasing) in the range from 52 to 90. The center of the array is located at [2500, 0, −5000] while the target is located at [4000, 0, 3000]. The resolution figure in figures 2–4 and 9 is defined as the distance from the target where the value $|\mathbb{E}u|$ has dropped to half of its target value.

In summary, in the ideal case where the noise and uncertainty are absent, the mean inverse filter has the best resolution performance which is independent of $C(0)$. But the mean inverse filter is not practical as it requires the accurate form of the mean transfer function (the frequency dependence of amplitude attenuation, in particular). Hence the uncertainty in the model and environment tends to spoil the performance due to the exponential growth factor in (13).

Both the mean-phase-matched filter and the (phase-matched) free-space propagator have similar resolution performance, require only the phase information of the mean transfer function and thus appear to be practical choices for imaging. However, the proximity of their resolutions is due to the parabolic nature of the cluttered medium and the scale of the plots. As demonstrated for the discrete model below, without the parabolic approximation

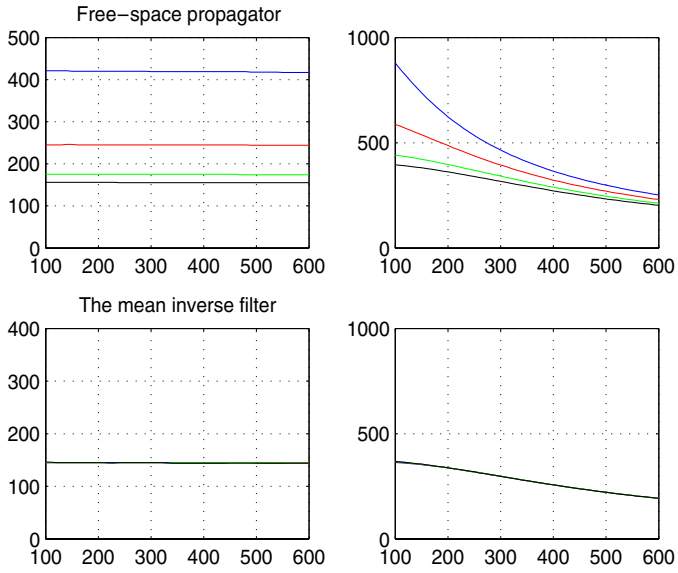

Figure 3. Longitudinal (left column) and transverse (right column) resolution of the parabolic Markovian model with the phase-matched free-space propagator and inverse filter and various extinction coefficients. The blue (full), red (dashed), green (dotted) and black (chain) curves represent, respectively, $C(0) = 0.16, 0.08, 0.04, 0.02$. The horizontal axis denotes the antenna spacing with five antennas.

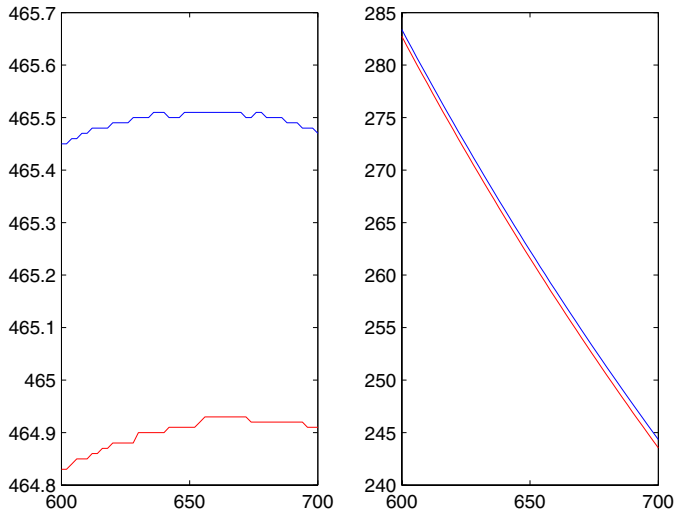

Figure 4. Longitudinal (left) and transverse (right) resolution with the free-space propagator as filter (blue full curve) and the mean-phase-matched filter (red dashed curve). The effective medium is defined by (20) with $\ell = 5 \times 10^{-5}\lambda^4$. The horizontal axis is the antenna spacing.

the resolution with the mean-phase-matched filter is slightly, but consistently, superior to that with the free-space propagator, see figure 4.

First let us digress to describe the mean transfer function of a random discrete model which will be used for the full imaging simulation.

5. Discrete model of randomly distributed point scatterers

We turn our attention to the discrete model for the following reasons: (i) the point scatterers are the simplest object to analyze the scattering of the *spherical* wave; (ii) second, application of point scatterers considerably simplifies multiple-scattering calculations needed, for instance, for understanding the optical properties of dense cold gases and optical lattices [7]; (iii) in the Inverse Synthetic Aperture Radar (ISAR) imaging, a point scatterer mechanism is frequently invoked, implicitly or explicitly.

For simplicity we will follow Twersky's theory as presented in [14] which is an effective medium theory. Unlike the parabolic Markovian model of the previous section, it is not mathematically rigorous.

Consider a *plane* wave incident on a single scatterer and let $f(\hat{\mathbf{o}}, \hat{\mathbf{i}}; \omega)$ be the scattering amplitude of the resulting scattered spherical wave with the incoming direction $\hat{\mathbf{i}}$ and outgoing direction $\hat{\mathbf{o}}$. In Twersky's theory the assumption of independent scattering is made and the Dyson equation for the coherent field reduces to the Foldy–Twersky integral equation

$$\bar{H}(\mathbf{x}, \mathbf{y}_m; \omega) = G_0(\mathbf{x}, \mathbf{y}_m; \omega) + \int f(\hat{\mathbf{o}}, \hat{\mathbf{i}}; \omega) G_0(\mathbf{x}, \mathbf{y}; \omega) \bar{H}(\mathbf{y}, \mathbf{y}_m; \omega) \rho(\mathbf{y})\, \mathrm{d}\mathbf{y},$$

where G_0 is the free-space propagator and ρ is the number density of scatterers. The modulus square of the scattering amplitude is the differential scattering cross section such that the scattering cross section σ_s is given by

$$\sigma_s = \int |f(\hat{\mathbf{o}}, \hat{\mathbf{i}}; \omega)|^2 \, \mathrm{d}\Omega(\hat{\mathbf{o}}). \tag{14}$$

The total (extinction) cross section σ_t is the sum of σ_s and the absorption cross section σ_a which is assumed zero. In the case of a *plane* wave incident on a scatterer, the forward-scattering theorem yields

$$\sigma_t = \begin{cases} \dfrac{4\pi}{k} \operatorname{Im}[f(\hat{\mathbf{i}}, \hat{\mathbf{i}}; \omega)], & d = 3 \\ 4 \operatorname{Im}[f(\hat{\mathbf{i}}, \hat{\mathbf{i}}; \omega)], & d = 2 \\ 2k \operatorname{Im}[f(\hat{\mathbf{i}}, \hat{\mathbf{i}}; \omega)], & d = 1 \end{cases} \tag{15}$$

[4, 13].

For uniformly distributed scatterers, with a constant density ρ, the coherent field in the high-frequency, forward-scattering approximation satisfies the effective equation

$$\left(\nabla^2 + K_{\mathrm{eff}}^2\right) \bar{H} = 0$$

with the effective wavenumber

$$K_{\mathrm{eff}} = k + 2\pi f(\hat{\mathbf{i}}, \hat{\mathbf{i}}; k) \rho / k. \tag{16}$$

The consequence of (15) and (16) is that the coherent field decays exponentially like (8)

$$\bar{H}(\mathbf{x}, \mathbf{y}; k) = -\mathrm{e}^{-\rho \sigma_t r/2} \frac{\mathrm{e}^{\mathrm{i} \operatorname{Re}[K_{\mathrm{eff}}] r}}{4\pi r}, \qquad r = |\mathbf{x} - \mathbf{y}|. \tag{17}$$

In most practical applications, the forward-scattering amplitude is nearly purely imaginary and the real part of the effective wave number is nearly the same as k. When the particle size a is much greater than the wavelength λ [19]

$$f(\theta) = \frac{\mathrm{i}a}{\sin\theta} J_1(ka \sin\theta) \tag{18}$$

where θ is the scattering angle between the incoming and outgoing directions. The forward-scattering amplitude is given by

$$\lim_{\theta\to 0} f(\theta) = \mathrm{i}\frac{ka^2}{2} \tag{19}$$

which yields $\sigma_t \approx 2\pi a^2$, according to the forward-scattering theorem (15). We then have

$$\bar{H}(\mathbf{x}, \mathbf{y}; k) = -\mathrm{e}^{-\frac{r}{2\ell}}\frac{\mathrm{e}^{\mathrm{i}kr}}{4\pi r}, \qquad r = |\mathbf{x} - \mathbf{y}|, \tag{20}$$

where

$$\ell = \frac{1}{\rho\sigma_t}$$

is the scattering mean-free path. In this case the total extinction cross section $\sigma_t \approx 2\pi a^2$ is independent of frequency, unlike in (8).

On the other hand, when the particle size is much smaller than the wavelength, the extinction cross section usually depends on the frequency as well. In the case of Rayleigh scattering without absorption, the scattering mean-free path scales like

$$\ell \sim \rho^{-1}k^{-4}a^{-6} \tag{21}$$

[16]. Similarly, in the case of the spatial white-noise refractive index fluctuation the mean-free path is given by

$$\ell = \frac{4\pi}{\gamma^2 k^4}, \tag{22}$$

where γ^2 is the intensity of the white-noise field, see, e.g. [1].

Now for the cluttered medium with the mean transfer function given by (20) the passive mode resolution performances of the mean-phase-matched filter and the free-space propagator are shown in figure 4. As before we calculate the resolutions in the noise-free case with (2), using the same 5-element array, same 20 frequencies and the same target location as in the parabolic model. The performance of the mean-phase-matched filter is consistently better than that of the free-space propagator, albeit the difference is small.

5.1. Numerical simulation with the Foldy–Lax formulation

We present the simulations of the discrete model of many point scatterers randomly distributed throughout the space.

This clutter model can be conveniently simulated in the Foldy–Lax formulation. Let the randomly distributed point scatterers of refractive index n_j be located at $\mathbf{x}_j$, $j = 1, 2, 3, \ldots, J$ and let $\Psi(\mathbf{x}; \omega_l)$ be the resulting wave field with the incident field $\Psi^{(\mathrm{in})}$. Then the Lippmann–Schwinger equation becomes in this case [16]

$$\Psi(\mathbf{x}; \omega_l) = \Psi^{(\mathrm{in})}(\mathbf{x}; \omega_l) + \sum_{j=1}^{J} \tau_j(\omega_l) G_0(\mathbf{x}, \mathbf{x}_j; \omega_l)\Psi(\mathbf{x}_j; \omega_l)$$

where G_0 is the Green function for the Helmholtz equation in the free space and the scattering strength τ_j of the jth scatterer is given by [7]

$$\tau_j(\omega_l) = \omega_l^2\left(n_j^2 - 1\right). \tag{23}$$

Once $\Psi(\mathbf{x}_i; \omega_l)$ are determined, they can be substituted in the Lippmann–Schwinger equation for the wave field at any location.

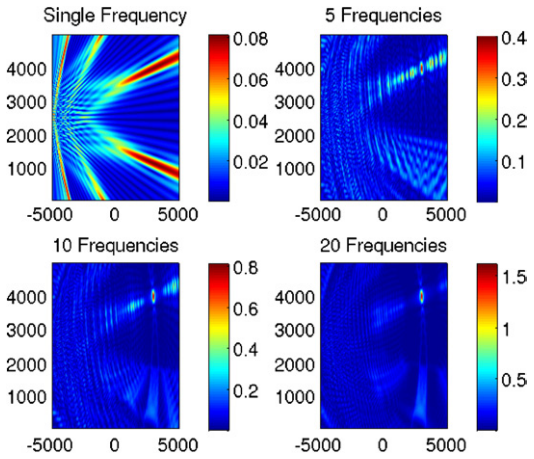

Figure 5. Passive array imaging $|u(\mathbf{x})|$ with 1, 5, 10 and 20 frequencies. The relative scattering strengths $n^2 - 1$ of each of the 3000 point scatterers and the target equal 70 and 1, respectively. The imaging result in the passive mode is, however, independent of the relative scattering strength of the target.

The Lippmann–Schwinger equation is valid for all $\mathbf{x}$ except at the actual scatterer locations $\mathbf{x} = \mathbf{x}_i$. So to determine $\Psi(\mathbf{x}_j; \omega_l)$ we replace the Lippmann–Schwinger equation by the Foldy–Lax equation

$$\Psi(\mathbf{x}_i; \omega_l) = \Psi^{(\text{in})}(\mathbf{x}_i; \omega_l) + \sum_{j \neq i} \tau_j(\omega_l) G_0(\mathbf{x}_i, \mathbf{x}_j; \omega_l) \Psi(\mathbf{x}_j; \omega_l), \tag{24}$$

where the divergent self-field term has been removed. Finding the field $\Psi(\mathbf{x}_i; \omega_l)$ is then reduced to inverting a matrix with entries

$$\delta_{ij} - (1 - \delta_{ij}) \tau_j(\omega_l) G_0(\mathbf{x}_i, \mathbf{x}_j; \omega_l), \qquad i, j = 1, 2, \ldots, J.$$

From $\Psi(\mathbf{x}_j; \omega_l)$ and the Lippmann–Schwinger equation we calculate the response matrix without the target(s). Similarly, the response matrix with the intrusion of target(s) can be calculated. We then apply the filter to the difference of the two response matrices, with and without the target(s).

For simplicity, we consider the case of identical point particles with $n_j = n, \forall\, j$. By the effective medium theory discussed in section 5 the mean transfer function decays with an increasing relative scattering strength $n^2 - 1$ and the density ρ of the particles. On the other hand, the magnitude of the fluctuations η, cf (1), increases with $n^2 - 1$ and ρ as can be seen from small τ asymptotic of the Foldy–Lax equation. In other words, the Rician factor decreases and the statistical stability deteriorates as $n^2 - 1$ and ρ increase. As a result, we expect the imaging performance to worsen accordingly. This is illustrated in figures 7 and 8.

In the simulations, either 1000 or 3000 point scatterers are uniformly randomly distributed in the domain $[2000, 4000] \times [0, 5000]$, while the whole computation domain is $[-5000, 5000] \times [0, 5000]$. The array of 11 antennas equally spaced is located on $x = -5000$ centered at $y = 2500$ with total aperture 2000. We use 1, 5, 10 and 20 equally spaced wavelengths from 52 to 90. In figures 5, 6, one point target is located at [3000, 4000] and in figures 7 and 8, there are seven targets located at [3100, 100], [2800, 1000], [4000, 1600], [3300, 2100], [4500, 3000], [3000, 4000] and [3500, 4800].

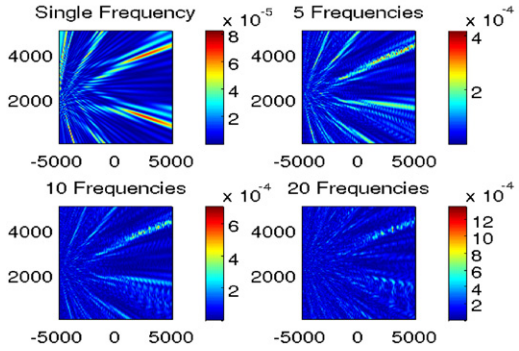

Figure 6. Active array imaging $|u(\mathbf{x})|$ with 1, 5, 10 and 20 frequencies. The relative scattering strengths $n^2 - 1$ of each of the 3000 point scatterers and the target equal 70 and 1, respectively.

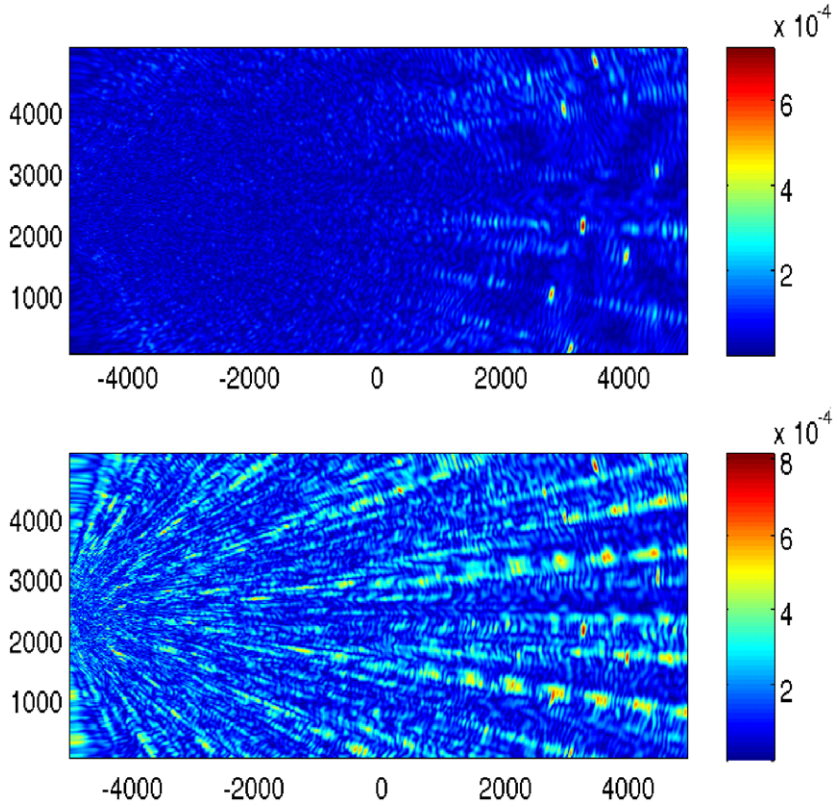

Figure 7. Active array imaging $|u(\mathbf{x})|$ of seven identical point targets with 20 frequencies. The relative scattering strengths $n^2 - 1$ of the scatterers and the targets equal 70 and 1, respectively. For the top and bottom plots, 1000 and 3000 particles are used, respectively.

When the contrast (ratio) between the scattering strength of the scatterers and the target is less than or equal to 70 (figures 5, 6), we see the improvement of stability and resolution as number of frequencies increases in both the passive and the active case. With one frequency, the imaging field exhibits spurious fluctuations which completely overshadow the target.

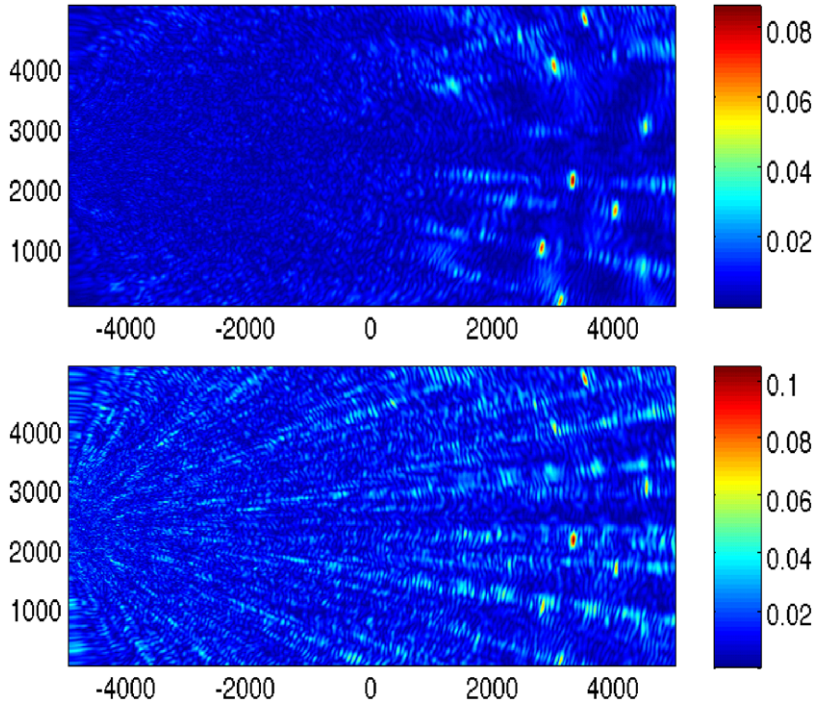

Figure 8. The same setting as in figure 7 except that the ω^{-1}-weighted mean-phase-matched filter is used. Compared to figure 7, the resolution worsens but the stability is improved.

With 10 or more frequencies the imaging field is relatively stable and the target shows up with good resolution. Comparing with the bottom right plot of figure 6 and the bottom plot of figure 7 we also see that the stability deteriorates as the number of targets increases.

When the clutter strength increases as the clutter scattering strength and the particle density increase, the imaging performance deteriorates accordingly, see figure 7. When the contrast (ratio) between the scatterers and the target increases to 100, the imaging performance deteriorates to the point that increasing the number of frequencies does not improve either stability or resolution (not shown here).

In figure 8 we experiment with the frequency-weight function ω^{-1}, namely we use the ω^{-1}-weighted mean-phase-matched filter

$$\omega^{-1}\,\mathrm{e}^{-\mathrm{i}kr},$$

cf (20). Compared to figure 7, this results in a slight deterioration of resolution but a significant improvement in stability, especially when the clutter strength is large. This can be explained by the fact that the ω^{-1} weight amplifies the influence of longer wavelengths and hence tends to stabilize but also smear the imaging result.

In figure 9, we compare the numerical resolution with the theoretical prediction based on the effective medium theory. We calculate the theoretical resolutions using (4) with (20) and the scattering mean-free-path

$$\ell = 0.01\lambda^4.$$

This particular ℓ is chosen to match the result of Foldy–Lax simulation. We see that the theoretical curves (red dashed) track closely those of the Foldy–Lax simulations (blue full).

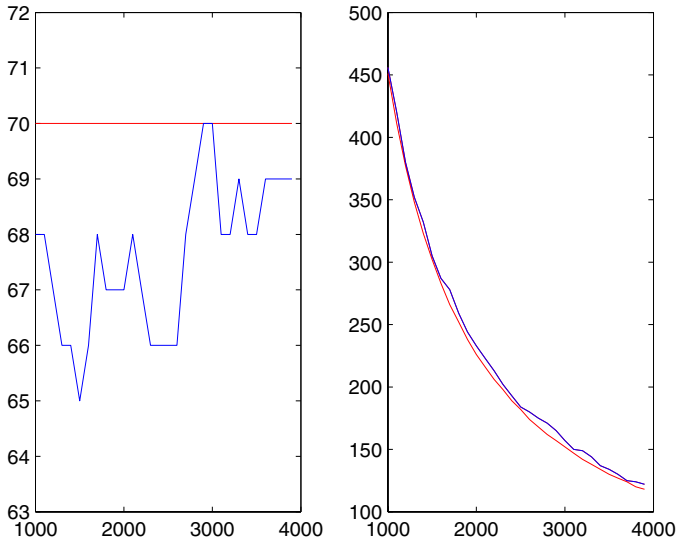

Figure 9. Resolutions with the mean-phase-matched filter. Longitudinal (left) and transverse (right) resolutions of active array imaging in the clutter (blue full curve) with 1000 particles and in the effective medium defined by (20) with $\ell = 0.01\lambda^4$ (red dashed curve) as a function of the *aperture*. The relative scattering strength $n^2 - 1$ of the scatterers and the targets equals 70 and 1, respectively. Note that the apparent 'choppiness' in the longitudinal resolution is due to the small range of the vertical scale.

6. Conclusions

In this paper we have derived a general condition $KBN \gg M$ under which the signal-to-interference ratio of the imaging functionals tends to infinity. This stability condition is valid in the Rician fading channels with sufficiently separated B frequencies, N antennas and M targets. In the case of the Rayleigh fading channel ($K \approx 0$) the imaging process should involve the cross correlation of responses and will be analyzed in a forthcoming paper.

We have used the theoretical results for the exactly solvable parabolic Markovian model to help identify reasonable filters. The mean-phase-matched filter is a practical choice and is subsequently used in the full imaging process with a discrete model of randomly distributed particles.

The effective medium theory for such a model provides an independent way of verifying our imaging theory: formulae (20) and (21) define an effective, noise-less medium for which the imaging resolution can be calculated in accordance with (2) or (4). Comparison with the simulation with the Foldy–Lax simulation shows consistent behavior to the k^{-4}-scaling of the mean-free path which characterizes the effective medium.

Acknowledgments

The research of ACF is supported in part by NSF grant DMS 0306659, DARPA grant N00014-02-1-0603. The research of PY is supported in part by DARPA grant N00014-02-1-0603.

Appendix A. Resolution analysis for the parabolic Markovian model

To facilitate explicit calculation let us assume that $d = 1$, $z_1 = \cdots = z_m$, that the frequency separation equals the coherence bandwidth β_c and the spacing of array elements equals the coherence length ℓ_c. We assume both β_c and ℓ_c are sufficiently small that the summation over ω_l and $y_n^\perp$ can be approximated by integrals. We consider the transverse resolution and set $z = z_1$. Note that the effective number of coherence bands $B \sim \beta_c^{-1}$ and $N \sim \ell_c^{-1}$.

A.1. The mean-matched filter

The spatial matched filter is basic to all imaging methods [15]. Since the exact matched filter is not known we consider the mean-matched filter (10).

Then the imaging field u has the mean

$$\mathbb{E}u(z, x^\perp) = \frac{1}{z^{1/2}2\pi} \sum_{m=1}^{M}\sum_{l=1}^{B}\sum_{n=1}^{N} \mathrm{e}^{-\omega_l^2 C(0)(z+z_1)/2}\omega_l^d z_1^{-d/2}\,\mathrm{e}^{-\mathrm{i}\omega_l(z_1-z)}\,\mathrm{e}^{-\mathrm{i}\frac{\omega_l\left|x^\perp-y_n^\perp\right|^2}{2z}}\,\mathrm{e}^{\mathrm{i}\frac{\omega_l\left|x_m^\perp-y_n^\perp\right|^2}{2z_1}}.$$

Let us write

$$\begin{aligned}\xi_{m,n} &= \frac{1}{2z_1}\left(\left|x^\perp - y_n^\perp\right|^2 - \left|x_m^\perp - y_n^\perp\right|^2\right)\\ &= \frac{1}{2z_1}\left(|x^\perp|^2 - \left|x_m^\perp\right|^2\right) + \frac{1}{z_1}\left(x_m^\perp - x^\perp\right)\cdot y_n\end{aligned}$$

so that

$$\begin{aligned}\sum_{n=1}^{N}\mathrm{e}^{-\mathrm{i}\frac{\omega_l\left|x^\perp-y_n^\perp\right|^2}{2z_1}}\,\mathrm{e}^{\mathrm{i}\frac{\omega_l\left|x_m^\perp-y_n^\perp\right|^2}{2z_1}} &\approx \frac{\mathrm{i}z_1}{\ell_c\omega_l\left(x_m^\perp - x^\perp\right)}\,\mathrm{e}^{-\mathrm{i}\frac{\omega_l}{2z_1}(|x^\perp|^2-|x_m^\perp|^2)}\\ &\quad\times\left(\mathrm{e}^{-\mathrm{i}\frac{\omega_l}{z_1}(x_m^\perp-x^\perp)\cdot y_{N+1}} - \mathrm{e}^{-\mathrm{i}\frac{\omega_l}{z_1}(x_m^\perp-x^\perp)\cdot y_1}\right)\end{aligned}$$

for sufficiently small ℓ_c. Assuming the bandwidth is sufficiently large (including negative frequencies) we then approximate the summation over ω_l by integration over $\omega \in (0, \infty)$ and obtain the approximation

$$\begin{aligned}\mathbb{E}u(z_1, x^\perp) &\approx \frac{\mathrm{i}}{\ell_c 2\pi}\sum_{m=1}^{M}\sum_{l=1}^{B}\mathrm{e}^{-\omega_l^2 C(0)z_1}\,\mathrm{e}^{-\mathrm{i}\frac{\omega_l}{2z_1}(|x^\perp|^2-|x_m^\perp|^2)}\,\frac{1}{x_m^\perp - x^\perp}\\ &\quad\times\left(\mathrm{e}^{-\frac{\mathrm{i}\omega_l}{z_1}(x_m^\perp-x^\perp)\cdot y_{N+1}} - \mathrm{e}^{-\frac{\mathrm{i}\omega_l}{z_1}(x_m^\perp-x^\perp)\cdot y_1}\right)\\ &\approx \frac{\mathrm{i}}{\ell_c\beta_c 2\pi}\sum_{m=1}^{M}\frac{1}{x_m^\perp - x^\perp}\int_0^\infty \mathrm{d}\omega\,\mathrm{e}^{-\omega^2 C(0)z_1}\,\mathrm{e}^{-\frac{\mathrm{i}\omega}{2z_1}(|x^\perp|^2-|x_m^\perp|^2)}\\ &\quad\times\left(\mathrm{e}^{-\frac{\mathrm{i}\omega}{z_1}(x_m^\perp-x^\perp)\cdot y_{N+1}} - \mathrm{e}^{-\frac{\mathrm{i}\omega}{z_1}(x_m^\perp-x^\perp)\cdot y_1}\right)\\ &\approx \frac{\mathrm{i}}{\ell_c\beta_c 2\pi}\sum_{m=1}^{M}\frac{1}{x_m^\perp - x^\perp}\int_0^\infty \mathrm{d}\omega\,\mathrm{e}^{-\omega^2 C(0)z_1}(\mathrm{e}^{-\mathrm{i}\omega\xi_{m,N+1}} - \mathrm{e}^{-\mathrm{i}\omega\xi_{m,1}}).\end{aligned} \tag{A.2}$$

In view of (A.1) the mean imaging function is a sum of localized functions centered at the M point targets. Provided that the targets are far apart so that the above summation over m is uniformly bounded with respect to M the above calculation shows that $\mathbb{E}u$ is of the order μBN since $B \sim \beta_c^{-1}$ and $N \sim \ell_c^{-1}$. Moreover the transverse resolution has the scaling behavior $\sqrt{C(0)z_1^3}$ as can be determined from the Fourier cosine and sine integrals in (A.2) by rescaling the integrating variable ω and the value $\mathbb{E}u\left(z_1, x_j^\perp\right)$ at the jth target is roughly proportional

to the total aperture $|y_{N+1} - y_1|$. The same analysis is also applicable to the next two filters discussed below.

A.2. The mean-phase-matched filter

Next we consider the phase-matched filter (11) which only incorporates the phase information of the mean propagator.

Then the imaging field u has the mean

$$\mathbb{E}u(z, x^\perp) = \frac{1}{(2\pi)^{1/2}} \sum_{m=1}^{M} \sum_{l=1}^{B} \sum_{n=1}^{N} \omega_l^{d/2} z_1^{-d/2} \, \mathrm{e}^{-\omega_l^2 C(0) z_1/2} \, \mathrm{e}^{-\mathrm{i}\omega_l (z_1 - z)} \, \mathrm{e}^{-\mathrm{i}\frac{\omega_l |x^\perp - y_n^\perp|^2}{2z}} \, \mathrm{e}^{\mathrm{i}\frac{\omega_l |x_m^\perp - y_n^\perp|^2}{2z_1}}$$

which, for $d = 1$, becomes approximately

$$\mathbb{E}u(z_1, x^\perp) \approx \frac{\mathrm{i}}{\ell_c \beta_c 2\pi} \sum_{m=1}^{M} \frac{1}{x_m^\perp - x^\perp} \int_0^\infty \mathrm{d}\omega \, \omega^{-1/2} \, \mathrm{e}^{-\omega^2 C(0) z_1/2} (\mathrm{e}^{-\mathrm{i}\omega \xi_{m,N+1}} - \mathrm{e}^{-\mathrm{i}\omega \xi_{m,1}}).$$

The same remark following (A.2) applies here as well.

A.3. The phase-matched free-space propagator

Consider the free-space parabolic propagator (12). The imaging field u has the mean

$$\mathbb{E}u(z, x^\perp) = \frac{1}{z^{1/2} 2\pi} \sum_{m=1}^{M} \sum_{l=1}^{B} \sum_{n=1}^{N} \omega_l z_1^{-1/2} \, \mathrm{e}^{-\omega_l^2 C(0) z_1/2} \, \mathrm{e}^{\mathrm{i}\omega_l (z_1 - z)} \, \mathrm{e}^{\mathrm{i}\frac{\omega_l |x^\perp - y_n^\perp|^2}{2z}} \, \mathrm{e}^{-\mathrm{i}\frac{\omega_l |x_m^\perp - y_n^\perp|^2}{2z_1}} \tag{A.3}$$

and hence for $d = 1$

$$\begin{aligned}\mathbb{E}u(z_1, x^\perp) &= \frac{1}{z_1 2\pi} \sum_{m=1}^{M} \sum_{l=1}^{B} \sum_{n=1}^{N} \omega_l \, \mathrm{e}^{-\omega_l^2 C(0) z_1/2} \, \mathrm{e}^{\mathrm{i}\frac{\omega_l |x^\perp - y_n^\perp|^2}{2z_1}} \, \mathrm{e}^{-\mathrm{i}\frac{\omega_l |x_m^\perp - y_n^\perp|^2}{2z_1}} \\ &\approx \frac{1}{z_1 2\pi} \sum_{m=1}^{M} \frac{1}{x_m^\perp - x^\perp} \int_0^\infty \mathrm{d}\omega \, \mathrm{e}^{-\omega^2 C(0) z_1/2} (\mathrm{e}^{\mathrm{i}\omega \xi_{m,N+1}} - \mathrm{e}^{\mathrm{i}\omega \xi_{m,1}}).\end{aligned}$$

As before, the same remark following (A.2) applies here.

A.4. The mean inverse filter

For the mean inverse filter (13) the imaging field u has the mean

$$\mathbb{E}u(z, x^\perp) = \sum_{m=1}^{M} \sum_{l=1}^{B} \sum_{n=1}^{N} \frac{\omega_l}{z^{1/2} z_1^{1/2}} \, \mathrm{e}^{\omega_l^2 C(0)(z - z_1)/2} \, \mathrm{e}^{-\mathrm{i}\omega_l (z_1 - z)} \, \mathrm{e}^{-\mathrm{i}\frac{\omega_l |x^\perp - y_n^\perp|^2}{2z}} \, \mathrm{e}^{\mathrm{i}\frac{\omega_l |x_m^\perp - y_n^\perp|^2}{2z_1}}. \tag{A.4}$$

Setting $z = z_1$ and approximating the summation over $\mathbf{y}_n^\perp$ by integration we obtain

$$\begin{aligned}\mathbb{E}u(z_1, x^\perp) &\approx \frac{\mathrm{i}}{\ell_c 2\pi} \sum_{m=1}^{M} \frac{1}{x_m^\perp - x^\perp} \sum_{l=1}^{B} \mathrm{e}^{-\frac{\mathrm{i}\omega_l}{2z_1}(|x^\perp|^2 - |x_m^\perp|^2)} \left(\mathrm{e}^{-\frac{\mathrm{i}\omega_l}{z_1}(x_m^\perp - x^\perp)\cdot y_{N+1}} - \mathrm{e}^{-\frac{\mathrm{i}\omega_l}{z_1}(x_m^\perp - x^\perp)\cdot y_1}\right) \\ &= \frac{\mathrm{i}}{\ell_c 2\pi} \sum_{m=1}^{M} \frac{1}{x_m^\perp - x^\perp} \left(\frac{\mathrm{e}^{-\mathrm{i}\omega_1 \xi_{m,N+1}} - \mathrm{e}^{-\mathrm{i}(\omega_B + \beta_c)\xi_{m,N+1}}}{1 - \mathrm{e}^{-\mathrm{i}\beta_c \xi_{m,N+1}}} - \frac{\mathrm{e}^{-\mathrm{i}\omega_1 \xi_{m,1}} - \mathrm{e}^{-\mathrm{i}(\omega_B + \beta_c)\xi_{m,1}}}{1 - \mathrm{e}^{-\mathrm{i}\beta_c \xi_{m,1}}} \right) \\ &\approx \frac{1}{\beta_c \ell_c 2\pi} \sum_{m=1}^{M} \frac{1}{x_m^\perp - x^\perp} \left(\frac{\mathrm{e}^{-\mathrm{i}\omega_1 \xi_{m,N+1}} (1 - \mathrm{e}^{-\mathrm{i}B\beta_c \xi_{m,N+1}})}{\xi_{m,N+1}} - \frac{\mathrm{e}^{-\mathrm{i}\omega_1 \xi_{m,1}} (1 - \mathrm{e}^{-\mathrm{i}B\beta_c \xi_{m,1}})}{\xi_{m,1}} \right)\end{aligned}$$

with $\xi_{m,n}$ given by (A.1). Note here we do not approximate the summation over ω_l by an integral as in the other cases.

For sufficiently separated target locations $x_m^\perp$ the summation over $x_m^\perp$ is uniformly bounded with respect to M but the summand, unlike the previous cases, is oscillatory and decays slowly. Nevertheless, $\mathbb{E}u$ again is of the order μBN. The resolution is independent of $C(0)$ but inversely depends on the total bandwidth $B\beta_c$. This implies that the resolution with the mean inverse filter can be indefinitely improved by increasing the bandwidth whereas in the other cases the resolution saturates as the bandwidth tends to infinity. The caveat is that the mean inverse filter (13), containing the exponential growth factor, is sensitive to the presence of noise.

A.5. Kolmogorov–Wiener filter

In the presence of additive white-Gaussian noise (AWGN), the optimum filter is the Kolmogorov–Wiener filter

$$P(z, x^\perp, y^\perp; \omega_l) = \frac{\bar{H}^*(z, x^\perp, y^\perp; \omega_l)}{|\bar{H}|^2(z, x^\perp, y^\perp; \omega_l) + \mathrm{SSNR}^{-1}(\omega_l)}, \tag{A.5}$$

where $\mathrm{SSNR}(\omega)$ is the spectral signal-to-noise ratio (SSNR), defined as the ratio of signal power to noise power at frequency ω.

Let σ be the noise power for all ω. Since the signal power is $\mathrm{e}^{-\omega_l^2 C(0)z}$, the Kolmogorov–Wiener filter can be written as

$$P(z, x^\perp, y^\perp; \omega_l) = \frac{\omega^{1/2}}{(2\pi \mathrm{i} z)^{1/2}} \left(\mathrm{e}^{-\omega_l^2 C(0)z/2} + \mathrm{e}^{3\omega_l^2 C(0)z/2}\sigma\right)^{-1} \mathrm{e}^{\mathrm{i}\omega_l z}\, \mathrm{e}^{-\mathrm{i}\frac{\omega_l |x^\perp - y^\perp|^2}{2z}}.$$

The Kolmogorov–Wiener filter is an ideal filter and it is difficult to realize in practice because first we must know the exact $\mathrm{SSNR}(\omega)$ and second slight changes in the noise or signal level could change the output signal drastically. A more stable alternative is to replace SSNR in (A.5) by a number that is considerably smaller than the minimum value of SSNR in the passband of interest. Such a filter is called a *pseudo-inverse filter* [15]. The pseudo-inverse filter with overestimated uncertainty eventually compromises the resolution performance.

References

[1] Akkermans E and Montambaux G 2003 Coherent effects in the multiple scattering of light in random media *Wave Scattering in Complex Media: From Theory to Applications (NATO Science Series)* ed B A van Tiggelen and S Skipetrov (Dordrecht: Kluwer)

[2] Borcea L, Tsogka C and Papanicolaou G 2003 Theory and applications of time reversal and interferometric imaging *Inverse Problems* **19** S139–64

[3] Borcea L, Tsogka C, Papanicolaou G and Berryman J 2002 Imaging and time reversal in random media *Inverse Problems* **18** 1247–79

[4] Carney P S, Schotland J C and Wolf E 2004 Generalized optical theorem for reflection, transmission and extinction of power for scalar fields *Phys. Rev.* E **70** 036611

[5] Dennison M L and Devaney A J 2004 Inverse scattering in inhomogeneous background media: II. Multi-frequency case and SVD formulation *Inverse Problems* **20** 1307–24

[6] Devaney A J, Marengo E A and Gruber F K 2005 Time-reversal-based imaging and inverse scattering of multiply scattering point targets *J. Acoust. Soc. Am.* **118** 3129–38

[7] de Vries P, van Coevorden D V and Lagendijk A 1998 Point scatterers for classical waves *Rev. Mod. Phys.* **70** 447–66

[8] Durgin G D 2003 *Space-Time Wireless Channels* (New Jersey: Prentice-Hall)

[9] Fannjiang A C 2005 White-noise and geometrical optics limits of Wigner–Moyal equation for beam waves in turbulent media II. Two-frequency formulation *J. Stat. Phys.* **120** 543–86

[10] Fannjiang A C 2006 Time reversal communication in Rayleigh fading broadcast channels with pinholes *Phys. Lett.* A **353/5** 389–97
[11] Fannjiang A C 2006 Information transfer in disordered media by broadband time reversal: stability, resolution and capacity *Nonlinearity* **19** 2425–39
[12] Fannjiang A C and Solna K 2005 Superresolution and duality for time reversal of waves in random media *Phys. Lett.* A **352** 22–9
[13] Ishimaru A 1978 *Wave Propagation and Scattering in Random Media* vol 1 (New York: Academic)
[14] Ishimaru A 1978 *Wave Propagation and Scattering in Random Media* vol 2 (New York: Academic)
[15] Kino G S 1987 *Acoustic Waves—Devices, Imaging and Analog Signal Processing* (Englewood Cliffs, NJ: Prentice-Hall)
[16] Newton R G 1982 *Scattering Theory of Waves and Particles* 2nd edn (New York: Dover)
[17] Prada C and Fink M 1994 Eigenmodes of the time-reversal operator: a solution to selective focusing in multiple target media *Wave Motion* **20** 151–63
[18] Proakis J G 2001 *Digital Communications* 4th edn (New York: McGraw-Hill)
[19] Van der Hulst H C 1981 *Light Scattering by Small Particles* (New York: Dover)